# Coexistence and Transition between Shear Zones in Slow Granular Flows

Robabeh Moosavi,[1] M. Reza Shaebani,[2,3] Maniya Maleki,[1] János Török,[4] Dietrich E. Wolf,[2] and Wolfgang Losert[5]

[1]*Department of Physics, Institute for Advanced Studies in Basic Sciences, Zanjan 45137-66731, Iran*
[2]*Computational Physics Group, University of Duisburg-Essen, D-47048 Duisburg, Germany*
[3]*Department of Theoretical Physics, Saarland University, D-66041 Saarbrücken, Germany*
[4]*Department of Theoretical Physics, Budapest University of Technology and Economics, Budapest H-1111, Hungary*
[5]*Department of Physics, University of Maryland, College Park, Maryland 20742, USA*

(Received 11 December 2012; published 3 October 2013)

We report experiments on slow granular flows in a split-bottom Couette cell that show novel strain localization features. Nontrivial flow profiles have been observed which are shown to be the consequence of simultaneous formation of shear zones in the bulk and at the boundaries. The fluctuating band model based on a minimization principle can be fitted to the experiments over a large variation of morphology and filling height with one single fit parameter, the relative friction coefficient $\mu_{\mathrm{rel}}$ between wall and bulk. The possibility of multiple shear zone formation is controlled by $\mu_{\mathrm{rel}}$. Moreover, we observe that the symmetry of an initial state, with coexisting shear zones at both side walls, breaks spontaneously below a threshold value of the shear velocity. A dynamical transition between two asymmetric flow states happens over a characteristic time scale which depends on the shear strength.

DOI: 10.1103/PhysRevLett.111.148301 PACS numbers: 47.57.Gc, 45.70.Mg, 83.50.Ax, 83.80.Fg

The intriguing rheology of granular materials has been widely studied over the years for its fundamental scientific interest and industrial and geophysical importance [1–3]. Shear banding is a widespread phenomenon in slow flows of complex materials, ranging from foams [4] and emulsions [5] to colloids [6] and granular matter [2,7–19]. A clear understanding of how the strain is localized and the material yields is crucial in order to develop a consistent continuum theory at low inertial numbers, which is currently an important open issue [10,20,21].

Slowly sheared granular materials usually develop narrow shear zones, often localized near a boundary, e.g., in avalanches [7], geological faults [8], and Couette flows [9–12], to mention a few. The characteristic length scale of the flow gradient is independent of the shear rate, ranges up to few particle diameters, and depends on particle shape and properties [9,10]. An important question we address is whether the formation of boundary-localized shear zones is intrinsic to granular matter or whether it can be prevented or controlled by suitable boundary conditions. Note that wide shear zones in granular bulk flow have been created, in a modified split-bottom Couette cell [13–15]. The emerging flow profiles were found to have shear zones tens of particle diameters wide. The wide shear zones were found to obey a number of scaling laws, with a transition from a shear zone near the surface at low filling heights to a closed cupola shape at high filling heights. It has not been clear, so far, whether or under what conditions the coexistence of these wide shear zones with the boundary-localized ones is possible and what happens to the universality of the flow profiles when dealing with more complex boundary conditions.

In slow flows, i.e., the state with rate-independent stresses, one expects that the steady-state flow pattern remains stable. One of the major findings of the present study is that the above concept does not work at shear velocities below a critical value.

In this Letter, we report on the experimental and numerical study of complex shear zone formation in a Couette cell geometry in which the split at the bottom is located at the outer cylinder (see Fig. 1). We show that the surface flow patterns can be explained by the linear combination of three distinct shear zones. Their existence is explained by a model based on an optimization principle which was already applied to shear zone formation in

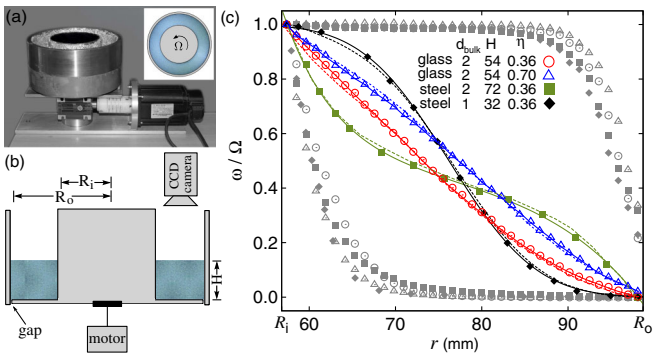


FIG. 1 (color online). (a) The experimental setup and its top view (inset). (b) Schematic of the side view. $R_i = 57$ mm and $R_o = 99$ mm. (c) Velocity profiles at different values of $H$ and $d_{\mathrm{bulk}}$ (in mm), and $\eta$. Symbols are experimental data, dashed curves are obtained from the variational approach [Eq. (1)], and solid curves are the fits with Eq. (3). The gray color denotes the localized profiles at the two extreme limits of $H$.

 

granular materials [16–19]. The relative magnitude of the bulk and wall effective friction coefficients turns out to be the key control parameter which determines the possibility of simultaneous formation of shear zones in the system and, hence, the overall shape of the flow profiles. More interestingly, upon decreasing the driving strength below a critical value $\Omega_c$, we observe a dynamical transition between boundary-localized shear zones.

*Setup.*—The experimental setup is shown in Fig. 1, with the inner and outer radii $R_i$ and $R_o$, respectively. The bottom plate and the inner cylinder of the apparatus rotate while the outer wall remains at rest. The cylindrical gap between the moving and standing parts has a size ($< 400$ $\mu$m) much smaller than the typical grain size, so that no particle can escape. The apparatus was filled up to height $H$ with spherical glass or steel beads of average diameter 0.5, 1, 2, or 3 mm with size polydispersity of about 15%. A layer of grains is glued to the bottom and side walls to obtain rough boundaries. The size polydispersity ensures that the flow profiles near the walls are not influenced by the ordering of grains [9,22]. While the bulk and boundary beads are always chosen of the same material, their size ratio $\delta = d_{\text{wall}}/d_{\text{bulk}}$ was varied in order to investigate the impact of the relative boundary roughness $\eta$ which is defined by the normalized penetration of the flowing particles into the rough surface as $\eta = 1 + \delta - \sqrt{1 + 2\delta - \delta^2/3}$ [23,24]. For smooth walls, $\eta = 0$.

*Velocity profiles.*—The inner cylinder and the comoving bottom plate are rotated at angular velocity $\Omega$. To avoid rate-dependent stresses [25], a gear is used to decrease the rotating shaft speed down to the range $0.05$ rad/s $< \Omega <$ $0.15$ rad/s, where the steady-state velocities are proportional to $\Omega$. Here, we show results for $\Omega = 0.15$ rad/s. The resulting surface flow is monitored from above using a fast CCD camera with pixel resolution 70 $\mu$m at a frame rate of 60 $s^{-1}$. The average angular velocity $\omega(r)$ at the free top surface is obtained by means of the particle image velocimetry method, which determines the average angular cross-correlation function in terms of the radial coordinate $r$ for temporally separated frames. After the flow reaches a steady state (generally in a few seconds), we measure $\omega(r)$ at the free surface as a function of $r$. The flow is wall localized for very shallow ($H \to 0$) and deep [$3(R_o - R_i) < H$] layers, with exponentially decaying strain rates. However, a rich variety of surface flow patterns can be observed in the middle range of $H$ [see Figs. 1(c) and 2(a)]; the profile shapes strongly depend on the choice of $H$, $\eta$, and material properties. The basic question is, how does the system adopt a stationary velocity profile?

*Variational approach.*—To provide physical insight into what determines the flow profile shape, we use a variational minimization procedure [26]. This method has been successfully applied to predict the closed cupola forms of shearing regions in deep granular beds [14–17] and the refraction of shear zones in layered granular materials

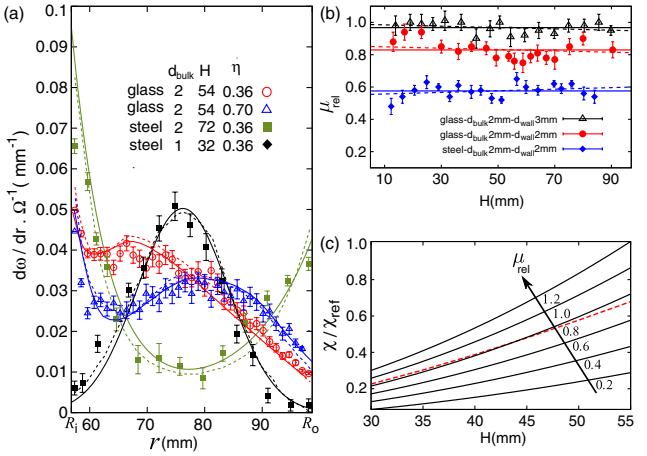


FIG. 2 (color online). (a) Radial dependence of the strain rate. The same symbols and lines as in Fig. 1(c) are used. (b) $\mu_{\text{rel}}$ obtained from the best fit of Eq. (1) to the data at different $H$. The horizontal solid lines indicate the mean values, and the dashed lines are the best linear fits. (c) The rate of energy dissipation $\chi$, scaled by the maximum dissipation of the bulk profile $\chi_{\text{ref}}$, versus $H$. The dissipation of the wide shear zone (dashed line) is compared to that of the localized shear zone at the outer cylinder at different values of $\mu_{\text{rel}}$ (solid lines).

[18,19,27]. Dry granular materials are best described by the Mohr-Coulomb theory, which limits the shear stress divided by the normal stress by the effective friction coefficient $\mu_{\text{eff}}$ of the material. Once the stress ratio exceeds $\mu_{\text{eff}}$, the material fails and a shear band forms. Because of cylindrical symmetry, the whole system can be described by a two-dimensional radial cut. The resulting shear band must be compatible with the boundary conditions and it should be the one which fails under the least torque or equivalently under the least dissipation rate. The last criterion can be formulated as

$$\int_0^H \mu_{\text{eff}} r(h)^2 (H - h) \sqrt{1 + (dr/dh)^2}\, dh = \min, \qquad (1)$$

where we search for the $r(h)$ function, i.e., the shear band position in the bulk of material at a given height $h$. Here, we used hydrostatic pressure since the Janssen effect plays no role due to the constant agitation of the driving [28].

The above plastic event (i.e., the instantaneous shear band) modifies the structure of the material in its vicinity. Hence, due to local fluctuations, another shear band can be optimal in the next instance. This is thus a self-organized process, where the shear band appears as a global optimum which itself modifies the medium in which the optimization is carried out. This is incorporated in a kinetic elastoplastic theory [20] which takes such self-organization into account. However, it is impossible to solve the model for the geometry of our problem; therefore, we use a fluctuating band model. The details of this model can be found in Ref. [17]; here, we reiterate only the main points. The two-dimensional cut is coarse grained (coarse graining length

can be as small as the particle diameter) into small mesoscopic cells which are characterized by a local effective friction coefficient. The friction coefficient is different in the bulk $\mu_{\rm eff}^{\rm bulk}$ and at the wall $\mu_{\rm eff}^{\rm wall}$ due to differences in texture. The actual strength of a particular cell in the bulk (at the wall) is chosen randomly from the interval $[0, \mu_{\rm eff}^{\rm bulk}]$ ($[0, \mu_{\rm eff}^{\rm wall}]$). An instantaneous shear band is chosen by minimizing Eq. (1). In the scope of this model, the width of this shear band is considered to be only one cell wide. Once the shear band is found, the local strength along it and in its neighborhood (next neighbor sites) are updated randomly. Shear profiles are obtained by an ensemble average over instantaneous slips. We note the following. (i) The actual probability distribution of $\mu_{\rm eff}$ [29] is not important in itself. The central limit theorem ensures that only its average and variance play a role in the integral of Eq. (1). (ii) The model has other parameters which are fixed by the geometry using the coarse graining length of a particle diameter size. The only free parameter we can vary for a given test is the ratio of the friction coefficients of wall and bulk $\mu_{\rm rel} = \mu_{\rm eff}^{\rm wall}/\mu_{\rm eff}^{\rm bulk}$.

The numerical velocity profiles obtained by tuning the single free parameter $\mu_{\rm rel}$ match remarkably with the experimental data, as shown in Figs. 1(c) and 2(a), given the fact that the boundary roughness is nonuniform, and size polydispersity would also influence the mechanical properties [30]. For a given set of bulk and wall particle sizes, the corresponding values of $\mu_{\rm rel}$ at different filling heights are obtained from the best fit to the experimental data with Eq. (1) within 7% error, showing that $\mu_{\rm rel}$ is roughly invariant with $H$ [Fig. 2(b)]. The constant nature of $\mu_{\rm rel}$ indicates that the fluctuating band model captures the right physics behind the effect of the walls because $\mu_{\rm rel}$ is fixed by the material size and type on the wall and in the bulk; therefore, it should be the same for all filling heights for a given set of materials.

When looking at different strain rate profiles, up to three maxima can be observed, one in the middle and two at the boundaries. In the geometry of our setup, these are indeed the only feasible choices of shear zones which minimize the rate of energy dissipation. The competition between these types of minimal paths gives rise to a rich shear zone phase diagram. Roughly speaking, the energy dissipation along the shear zone at the outer cylinder is proportional to $\mu_{\rm eff}^{\rm wall} R_o^2 H^2$, while the cost of the path which sticks to the bottom plate and then to the inner cylinder grows with $\mu_{\rm eff}^{\rm wall}[R_i^2 H^2 + \frac{2}{3}(R_o^3 - R_i^3)H]$. Hence, one expects that the inner shear zone wins the race only above $H \sim 80$ mm. Assuming that the middle shear zone with the center position $R_w$ is the universal wide zone reported in Refs. [13–15], it should follow a path in the bulk of material which is given by [16]

$$h = H - r\left[1 - \frac{R_o}{r}[1 - (H/R_o)^{\alpha}]\right]^{1/\alpha}, \qquad (2)$$

and the total dissipation along the broad shear zone is equal to $2\pi\mu_{\rm eff}^{\rm bulk}\int_{R_w}^{R_o}(H-h)r^2\sqrt{1+(dh/dr)^2}dr$. The exponent $\alpha$ is introduced after Eq. (3). A comparison between this trajectory (within the range of $H$, it may exist) and the trajectory which sticks to the outer cylinder shows that the former becomes favorable only for $\mu_{\rm rel} \gtrsim 0.8$ [Fig. 2(c)]. After detailed calculations, Fig. 3 summarizes the results of the formation and coexistence of shear zones in a phase diagram in the ($\mu_{\rm rel}$, $H$) space. The numerical diagram reveals that the $H$ dependence of the surface profile shape has a nontrivial dependence on $\mu_{\rm rel}$. This has been confirmed by the experimental results, obtained for the accessible values of ($\mu_{\rm rel}$, $H$).

The model numerically reproduces the experiment well without providing an explicit analytical expression for the velocity profiles. In the following, we address whether a functional form can be proposed, based on the combination of possible basic ingredients: wall-localized shear zones with exponential flow profiles [9–12] and wide shear zones with Gaussian velocity gradient profiles [13,17]. We find that both all experimental and numerical profiles are well fitted by a superposition of a Gaussian and two exponential curves [solid lines in Figs. 1(c) and 2(a)]:

$$\frac{d\omega(r)}{dr} = a_i \exp[-b_i(r - R_i)] + a_o \exp[-b_o(R_o - r)] + \frac{a_w}{\sqrt{\pi}\xi}\exp[-(x - R_w)^2/\xi^2]. \qquad (3)$$

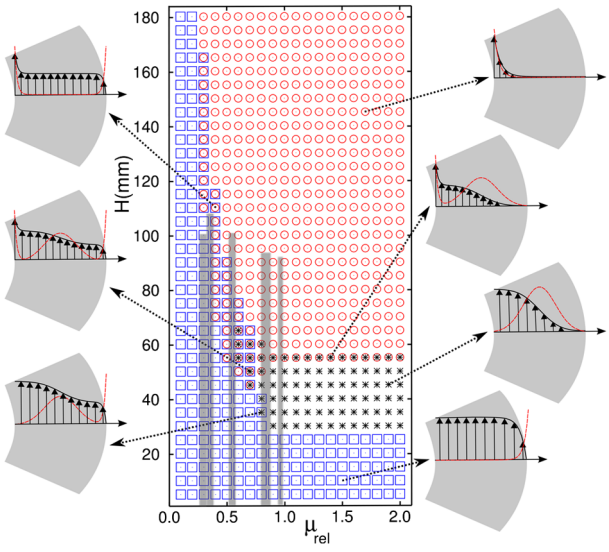


FIG. 3 (color online). Phase diagram of shear zone coexistence for $d_{\rm bulk} = 2$ mm. The squares, circles, and stars denote the shear zone at the outer and inner cylinders and in the bulk, respectively. The gray shaded regions denote the values of ($\mu_{\rm rel}$, $H$) for which the experiments are performed. Insets: Typical velocity fields (sketched with arrows) and the corresponding strain rates (red curves) (both corrected for the radial dependence).

The contribution of different terms evolves with $H$ in such a way that confirms the validity of the numerical phase diagram. Also, the universality of the wide shear zone is preserved; i.e., the evolution of the width $\xi$ and the center position $R_w$ of the wide zone follows, respectively, $H^{2/3}$ and $R_o[1-(H/R_o)^{\alpha}]$, compatible with prior work [13,15]. The exponent $\alpha$, however, ranges between 1.4 and 2.5. The discrepancy can be attributed to the relatively large $d_{\mathrm{bulk}}$ compared to the system size.

We find that our additional parameters, the characteristic lengths of the exponential decays $b_i$ and $b_o$, are influenced by the particle size and type. They evolve with the filling height in the following way: For a given experimental setting, $b_o$ scales with $H$ as $\exp(-\lambda_o H)$ [Fig. 4(a)]. The decay constant $\lambda_o$ grows weakly with increasing $\eta$, meaning that the larger roughness is accompanied by the faster suppression of the outer shear zone with increasing the filling height. The exponent $b_i$ shows a saturation behavior with $H$ [Fig. 4(b)], with the following empirical scaling relation

$$b_i(H)/b_i^{\infty} \sim \left(1+\tanh\left[\frac{H-H_o}{2w}\right]\right), \tag{4}$$

with $H_o$ and $w$ being the center and width of the hyperbolic tangent. The saturation value $b_i^{\infty}$ decays exponentially with $\eta$ for a given material (not shown). In short, the surface flow pattern is a linear combination of a few basic elements, each of which satisfies simple scaling laws.

We also determine the relation between $\mu_{\mathrm{rel}}$ and the boundary roughness $\eta$. As illustrated in Fig. 4(c), a clear dependency on the material type can be observed. One expects that $\mu_{\mathrm{rel}}$ saturates towards $\mu_{\mathrm{rel}}^{\infty}=1$ at $\eta\to\infty$, since the bulk particles fill the holes and smoothen the boundary roughness so that they practically roll over each other. The behavior at $\eta\to 0$ depends on material type and particle size. We attribute the particle size dependence to the roughness caused by the uneven gluing.

*Instability at low shear velocities.*—All the experimental results reported so far were obtained in the rate-independent regime $0.05\ \mathrm{rad/s} < \Omega < 0.15\ \mathrm{rad/s}$, where the flow profiles rapidly reach their final steady-state shapes. Let us consider a case with two coexisting shear zones at both side walls, obtained at $\eta = 0.36$ and by adjusting the height of the steel bead layer to $H \simeq 80$ mm. We observe an anomalous behavior, a spontaneous symmetry breaking of the flow profile, as the shear velocity is decreased below $\Omega_c \sim 5\times 10^{-3}$ rad/s (see Fig. 5). The system is found in either of the two asymmetric flow states with strain localization at only one boundary. A dynamical transition between the two states takes place over a characteristic time scale, which decays to zero at $\Omega\to\Omega_c$ ($\Omega<\Omega_c$). A similar asymmetric shear zone has been recently reported in experiments on colloidal glasses [31] (although with permanent rather than transient behavior) and in numerical simulations of plane shear flow [23]. Based on the analysis of velocity fluctuations, a plausible scenario is that the agitations induced by the external driving at shear velocities lower than $\Omega_c$ are not strong enough to trigger shear zones at both walls. Thus, the system is trapped in one of two minimal states. The shear rate plays the role of a kind of "temperature," enabling the system to visit both minimal states. When the system is sheared slower than $\Omega_c$, it freezes in one of the shear zone locations for a long time. As the shear velocity approaches $\Omega_c$, the switching happens more frequently, and the transition time goes to zero. Note that the velocity profiles in the small $\Omega$ state can also be recovered from the fluctuating band model when averaging over a long time window.

In conclusion, the possibility of multiple shear zones and the transitions between two of the most thoroughly investigated kinds of shear flow behaviors in dry granular materials is studied through careful comparison of experiment and modeling. We describe those aspects of the microstructure that are translated to the global rheology and verify that the formation of localized boundary shear zones is not an intrinsic property of granular matter. One can adjust the relative strength of bulk and boundary shear zones by tuning the relative effective friction. Tuning it via the boundary conditions and material properties, it is

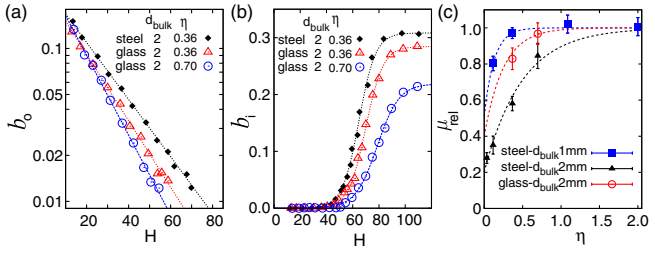


FIG. 4 (color online). (a),(b) Evolution of the decay exponents $b_o$ and $b_i$ with $H$. The lines indicate (a) exponential fits and (b) fits given by Eq. (4). (c) $\mu_{\mathrm{rel}}$ (averaged over all filling heights) versus the wall roughness $\eta$. The curves are exponential saturation fits as guides to the eye.

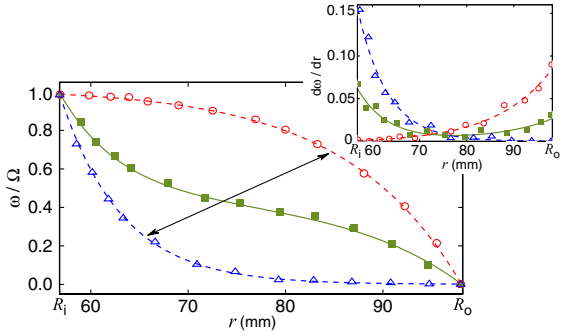


FIG. 5 (color online). The surface flow profile at $\Omega = 0.1$ rad/s (solid curve) and two typical profiles at $\Omega = 4\times 10^{-3}$ rad/s (dashed curves), and the corresponding strain rates (inset).

possible to either enhance or minimize boundary shear zones.

Our study may also be used as a template for a practical tool to measure the effective friction coefficient of the material from surface flow patterns. Our finding, that the minimization of energy dissipation governs the intriguing behavior, is a major step forward towards understanding the mechanisms of shear localization in granular materials, which is an outstanding challenge in the physics of complex flows, geophysics, and industry. The observed instabilities at low shear velocities deserve further detailed studies to uncover the underlying physics. The results of plane shear flows [23] suggest that the rotational degrees of freedom of particles play a crucial role in facilitating the dynamical transitions between the optimum states.

We would like to thank T. Unger and Z. Shojaaee for helpful discussions. R. M. and M. M. acknowledge the support of this project by the Institute for Advanced Studies in Basic Sciences (IASBS) Research Council under Grant No. G2010IASBS136, and M. R. S. and D. E. W. by DGF Grant No. Wo577/8-1 within the priority program ''Particles in Contact.'' W. L. acknowledges support from DTRA Grant No. 10DTRA1077, and J. T. from OTKA NN-107737.

[1] Y. Forterre and O. Pouliquen, Annu. Rev. Fluid Mech. **40**, 1 (2008); I. S. Aranson and L. S. Tsimring, Rev. Mod. Phys. **78**, 641 (2006).
[2] P. Schall and M. van Hecke, Annu. Rev. Fluid Mech. **42**, 67 (2010).
[3] R. Nedderman, *Statics and Kinematics of Granular Materials* (Cambridge University Press, Cambridge, England, 1992).
[4] R. Höhler and S. Cohen-Addad, J. Phys. Condens. Matter **17**, R1041 (2005); J. Lauridsen, G. Chanan, and M. Dennin, Phys. Rev. Lett. **93**, 018303 (2004); G. Katgert, M. E. Möbius, and M. van Hecke, Phys. Rev. Lett. **101**, 058301 (2008).
[5] L. Bécu, S. Manneville, and A. Colin, Phys. Rev. Lett. **96**, 138302 (2006); N. D. Denkov, S. Tcholakova, K. Golemanov, K. P. Ananthapadmanabhan, and A. Lips, Phys. Rev. Lett. **100**, 138301 (2008).
[6] J. K. G. Dhont, M. P. Lettinga, Z. Dogic, T. A. J. Lenstra, H. Wang, S. Rathgeber, P. Carletto, L. Willner, H. Frielinghaus, and P. Lindner, Faraday Discuss. **123**, 157 (2003); I. Cohen, B. Davidovitch, A. B. Schofield, M. P. Brenner, and D. A. Weitz, Phys. Rev. Lett. **97**, 215502 (2006); L. Isa, R. Besseling, and W. C. K. Poon, Phys. Rev. Lett. **98**, 198305 (2007).
[7] A. Daerr and S. Douady, Nature (London) **399**, 241 (1999); T. Börzsönyi, T. C. Halsey, and R. E. Ecke, Phys. Rev. Lett. **94**, 208001 (2005).
[8] D. R. Scott, Nature (London) **381**, 592 (1996); G. Gudehus and K. Nubel, Géotechnique **54**, 187 (2004).
[9] D. M. Mueth, G. F. Debregeas, G. S. Karczmar, P. J. Eng, S. R. Nagel, and H. M. Jaeger, Nature (London) **406**, 385 (2000).
[10] L. Bocquet, W. Losert, D. Schalk, T. C. Lubensky, and J. P. Gollub, Phys. Rev. E **65**, 011307 (2001).
[11] W. Losert, L. Bocquet, T. C. Lubensky, and J. P. Gollub, Phys. Rev. Lett. **85**, 1428 (2000).
[12] M. Latzel, S. Luding, H. J. Herrmann, D. W. Howell, and R. P. Behringer, Eur. Phys. J. E **11**, 325 (2003).
[13] D. Fenistein and M. van Hecke, Nature (London) **425**, 256 (2003).
[14] X. Cheng, J. Lechman, A. F. Barbero, G. Grest, H. Jaeger, G. Karczmar, M. Möbius, and S. Nagel, Phys. Rev. Lett. **96**, 038001 (2006).
[15] D. Fenistein, J. W. van de Meent, and M. van Hecke, Phys. Rev. Lett. **96**, 118001 (2006).
[16] T. Unger, J. Török, J. Kertesz, and D. E. Wolf, Phys. Rev. Lett. **92**, 214301 (2004).
[17] J. Török, T. Unger, J. Kertesz, and D. E. Wolf, Phys. Rev. E **75**, 011305 (2007).
[18] T. Unger, Phys. Rev. Lett. **98**, 018301 (2007).
[19] T. Börzsönyi, T. Unger, and B. Szabó, Phys. Rev. E **80**, 060302(R) (2009).
[20] L. Bocquet, A. Colin, and A. Ajdari, Phys. Rev. Lett. **103**, 036001 (2009).
[21] V. Mansard and A. Colin, Soft Matter **8**, 4025 (2012).
[22] G. Chambon, J. Schmittbuhl, A. Corfdir, J. P. Vilotte, and S. Roux, Phys. Rev. E **68**, 011304 (2003).
[23] Z. Shojaaee, L. Brendel, J. Török, and D. E. Wolf, Phys. Rev. E **86**, 011302 (2012).
[24] G. Koval, F. Chevoir, J.-N. Roux, J. Sulem, and A. Corfdir, Granular Matter **13**, 525 (2011).
[25] R. R. Hartley and R. P. Behringer, Nature (London) **421**, 928 (2003).
[26] L. Onsager, Phys. Rev. **37**, 405 (1931); **38**, 2265 (1931); R. Baker and M. Garber, Géotechnique **28**, 395 (1978); I. Einav and M. Randolph, Géotechnique **56**, 501 (2006).
[27] H. A. Knudsen and J. Bergli, Phys. Rev. Lett. **103**, 108301 (2009).
[28] K. Nichol, A. Zanin, R. Bastien, E. Wandersman, and M. van Hecke, Phys. Rev. Lett. **104**, 078302 (2010).
[29] M. R. Shaebani, T. Unger, and J. Kertész, Phys. Rev. E **78**, 011308 (2008).
[30] M. R. Shaebani, M. Madadi, S. Luding, and D. E. Wolf, Phys. Rev. E **85**, 011301 (2012).
[31] R. Besseling, L. Isa, P. Ballesta, G. Petekidis, M. E. Cates, and W. C. K. Poon, Phys. Rev. Lett. **105**, 268301 (2010).